Facile Synthesis and Chiral Resolution of Expanded Helicenes with up to 35 cata-Fused Benzene Rings

Gui-Fei Huo,[a]+ Toshiya M. Fukunaga,[b]+ Xudong Hou,[a] Yi Han,[a] Wei Fan,[a] Shaofei Wu,*[a] Hiroyuki Isobe,*[b] Jishan Wu*[a]

[a] Department of Chemistry, National University of Singapore, 3 Science Drive 3, 117543, Singapore E-mail: chmwuj@nus.edu.sg (J. W.); chmswu@nus.edu.sg (S.W.)
[b] Department of Chemistry, The University of Tokyo, Hongo, Bunkyo-ku, Tokyo 113-0033, Japan E-mail: isobe@chem.s.u-tokyo.ac.jp (H.I.)
+These authors contributed equally to this work

Abstract

Expanded helicenes are expected to show enhanced chiroptical properties as compared to the classical helicenes but the synthesis is very challenging. Herein, we report the facile synthesis of a series of expanded helicenes **Hn** (n=1-4) containing 11, 19, 27 and 35 *cata*-fused benzene rings through Suzuki coupling-based oligomerization followed by $Bi(OTf)_3$-mediated regioselective cyclization of vinyl ethers. Their structures were determined by X-ray crystallographic analysis. Enantiopure **H2**, **H3**, and **H4** can be isolated by chiral HPLC and they all exhibit strong chiroptical responses with high absorption dissymmetry factor ($|g_{abs}|$) values (0.020 for **H2**, 0.021 for **H3**, and 0.021-0.024 for **H4**).

Introduction

The classical helicenes contain angularly fused aromatic rings (Figure 1a) and express strong chiroptical responses due to their intrinsic helical chirality.[1] A logical approach to enhance the chiroptical properties is an elongation of the helical structure. However, synthesis of long helicenes is very challenging as it requires the introduction of large strain and regioselective fusion of many rings. So far, the longest helicene is a [16]helicene reported by Fujita et al.[2] Alternatively, multiply fused helicenes have been reported and many of them show improved chiroptical properties as compared to their single helicene counterparts.[3] Another way is to increase the size of a helicene by alternation of the linear and angular ring fusion, the so-called “expanded helicenes” approach (Figure 1a).[4] Such expansion could enhance the chiroptical properties due to more extended π-conjugation and modulation of the frontier molecular orbital symmetry and transition moments.[5] Synthesis of expanded helicenes is also challenging and several expanded helicenes have been reported in recent years by different synthetic methods (Figure 1b). For example, Tilley et al reported a tribenzo-, expanded [13]helicene (A) through a three-fold, partially intermolecular [2+2+2] cycloaddition with substrates containing three diyne units.[4] Matsuda et al synthesized a π-expanded helicene that is the helically twisted analogue of kekulene (B) by using a 6-fold ring-closing olefin metathesis reaction as a key step.[6] Toyota et al developed a series of expanded helicenes consisting of up to five fused anthracene units (C) by $PtCl_2$-catalyzed cycloisomerization.[7] However, the enantiomers of the abovementioned expanded helicenes could not be isolated by

chiral HPLC at room temperature due to their relatively low racemization barriers. Later, Yashima et al reported the facile synthesis of several consecutively fused expanded helicenes (D) through the trifluoroacetic acid-promoted intramolecular multistep cascade alkyne benzannulations.[8] Notably, the triple-expanded helicene (n=3) showed persistent chirality with the absorption and luminescence dissymmetry factors of up to 1.5 × 10^{-2} ($|g_{abs}|$) and 0.94 × 10^{-2} ($|g_{lum}|$), respectively. These studies imply promising chiroptical properties of expanded helicenes but the synthesis of even longer expanded helicenes remains very challenging. Recently, our groups demonstrated that $Bi(OTf)_3$-mediated cyclization of vinyl ethers was a very efficient benzannulation approach for the synthesis of cycloarenes,[9] expanded kekulenes,[10] and twisted carbon nanobelts.[11] We expect that such a reaction could be also used for the synthesis of expanded helicenes if appropriate precursors are designed. In this work, we report the facile synthesis of a series of expanded helicenes **Hn** (n=1-4) containing 11, 19, 27 and 35 *cata*-fused benzene rings (Figure 1b) through a synthetic strategy mainly involving Suzuki coupling followed by $Bi(OTf)_3$-mediated cyclization reaction. The enantiomers of the three longer expanded helicenes (**H2**-**H4**) were successfully isolated by chiral HPLC and they all showed high absorption dissymmetric factors.

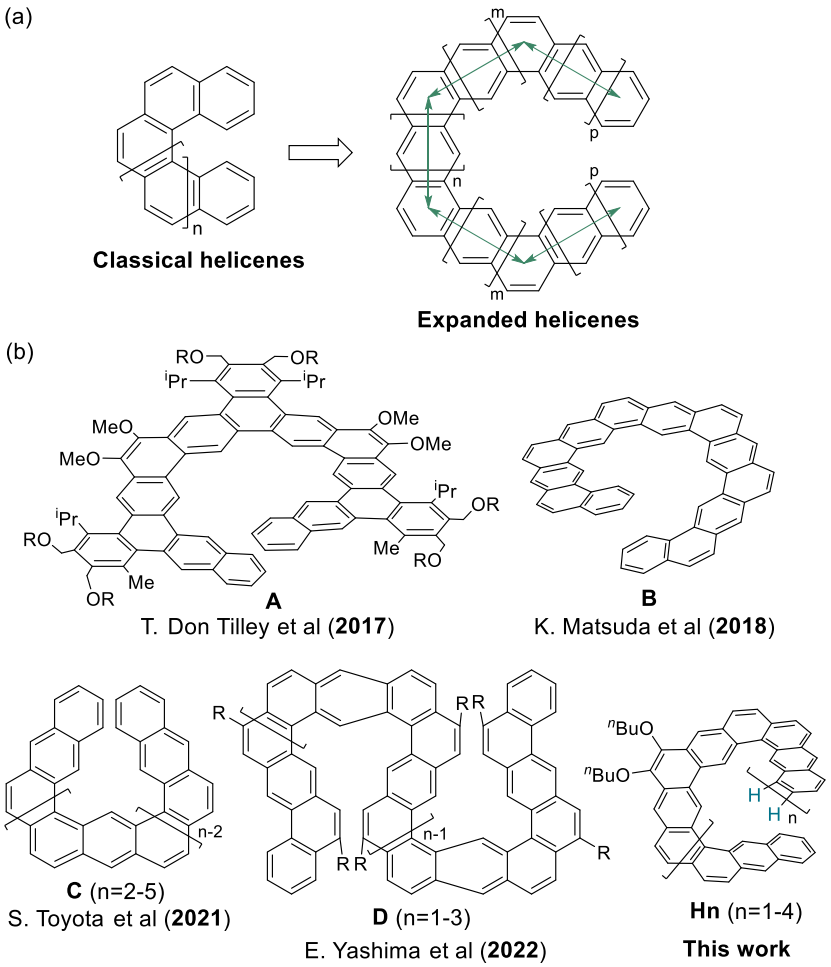

Figure 1. (a) The concept of from classical helicenes to expanded helicenes. (b) Representative examples of known expanded helicenes and the new expanded helicenes **Hn** (n = 1-4) reported in this work.

Results and Discussion

As shown in Scheme 1, two readily accessible building blocks, the 2,9-dibromo-phenanthrene **1**[12] carrying two vinyl ether groups and two solubilizing n-butoxy substituents, and the 1,8-anthracene derivative **2**[13] with two pinacol borate (Bpin) units, were subjected to Suzuki coupling reaction involving $Pd_2(dba)_3$, $[(^tBu)_3PH]BF_4$ and $NaHCO_3$ in THF/H_2O at 80 °C.[14] MALDI-TOF mass spectrometry analysis indicates the formation of a series of oligomers (**3**) with the terminal Bpin groups replaced by hydrogen atoms after 3 days. The crude product was extracted by dichloromethane (DCM), washed with water, and passed through a silica gel column. Without further purification, the mixture of the oligomer precursors **3** was subjected to $Bi(OTf)_3$-mediated cyclization reaction in 1,2-dichloroethane (DCE) at 60 °C for 8 hours, and the fully fused expanded helicenes **H1**-**H4** were isolated by preparative GPC in 33.3%, 13.5%, 4.1%, and 0.8% yield, respectively, over two steps. Their structures were unambiguously confirmed by X-ray crystallographic analysis (see below), NMR, and high-resolution mass spectrometry (see supporting information (SI)). The high regioselective cyclization could be due to the larger strain if the cyclization goes to the *meso*-carbon of the anthracene unit (formation of seven-membered ring) as compared to the *β*-carbons (formation of six-membered ring).

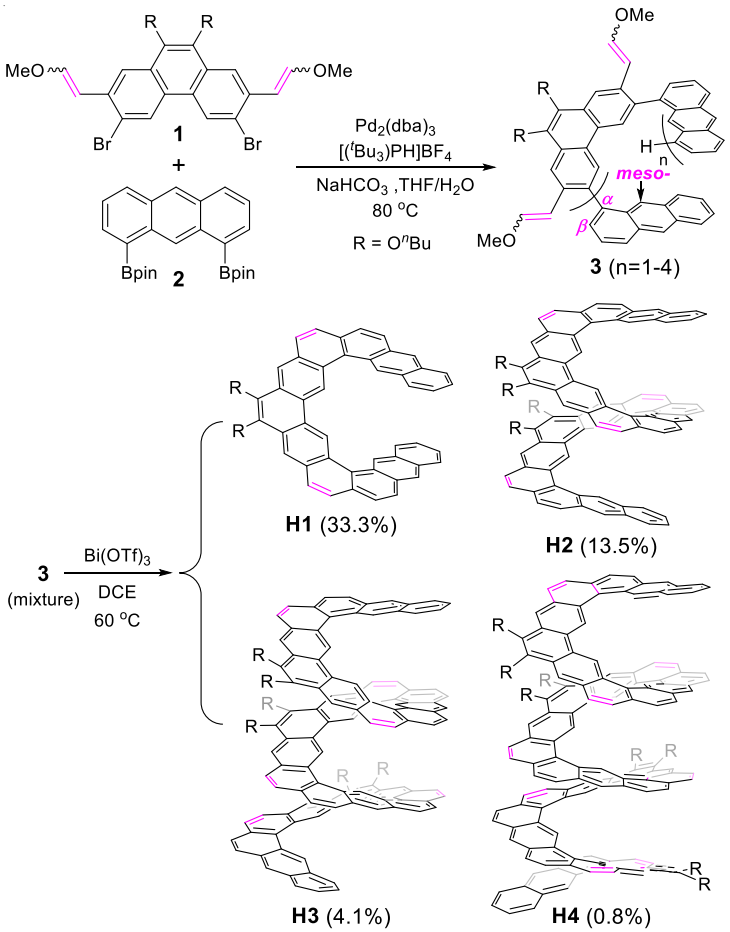

Scheme 1. Synthetic route of the expanded helicenes **H1**-**H4**.

Single crystals of **H1**, **H2**, **H3**, and **H4** were grown by slow solvent diffusion of methanol into their racemic solutions in DCM, DCM, toluene, and benzene, respectively.[15]

X-ray crystallographic analysis revealed that both (*P*) and (*M*) enantiomers co-existed in the crystal structure (Figure 2). In all cases, the expanded helicene architecture constitutes a supramolecular chiral column along the axis with an intermolecular π-π stacking. For **H1**, the two enantiomers are packed extremely compact via strong π-π interactions (d = 3.27-3.33 Å) into a one-dimensional (1D) polymer chain, and the chains are further packed into a three-dimensional (3D) structure with additional [CH…π] and van der Waals interactions (Figure 2b). The angle between the two planes of the terminal rings A and K (θ_{AK} = 5.7°) (Figure 2a) is significantly smaller than that of [7]helicene (θ = 32.8°),[16] indicating less strain in the expanded helicenes with a large helical diameter (d_h = 9.15 Å) (Figure S5 in SI). The crystallographic analysis of **H2** showed that only one of the enantiomers was packed into a long polymer chain (*P* chain or *M* chain) through close π-π contacts with distances of 3.32-3.40 Å, and each chiral chain exists independently (Figure 2d). The close intermolecular packing along the chain also results in a very small distortion angle θ_{AK} close to 0°. On the other hand, the angle (θ_{EO}) between the two spatially overlapped rings O and E is measured as about 22.27° due to larger strain (Figure 2c). **H3** displays a similar packing structure to that of **H1**, with close π-π interactions (d = 3.39 Å) between the neighboring *P*/*M* enantiomers in the individual column (Figure 2f). The angles θ_{AK} and θ_{EO} are measured as 0° and 14.42°, respectively (Figure 2e). For **H4**, *P*/*M* enantiomer pairs are identified in the molecular packing, where enantiomers with the same chirality (*P* or *M*) are packed in a columnar fashion via inter-molecular π-π interactions (d_1 = 3.36 Å, d_2 = 3.35 Å, and d_3 = 3.36 Å) (Figure 2h). The molecule makes about 3.5 turns, with angles θ_{AK} and θ_{EO} measured as 0° and 16.77°, respectively (Figure 2g).

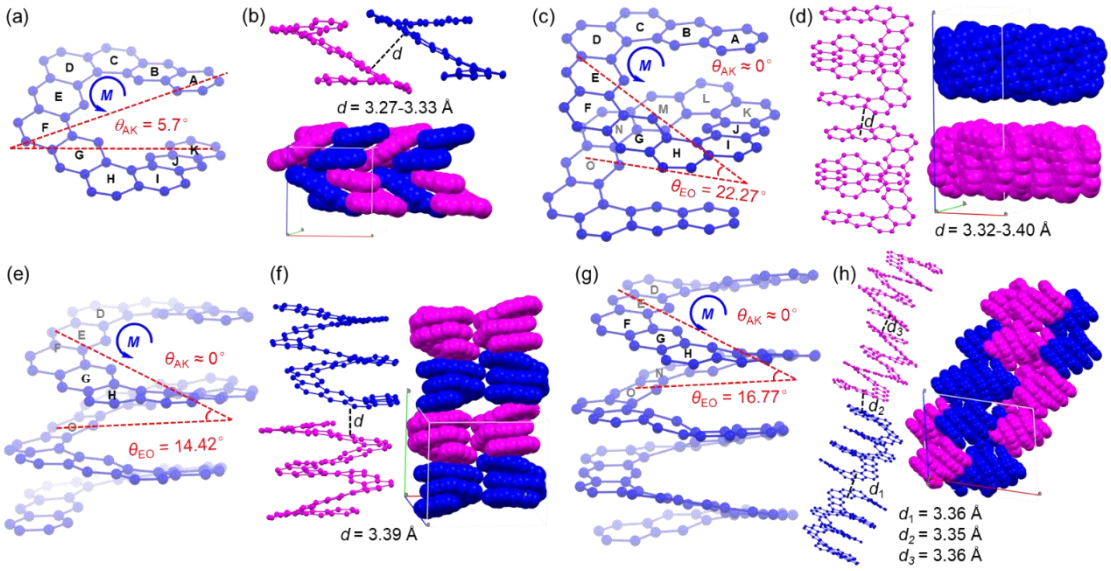

Figure 2. X-ray crystallographic structures of **H1**-**H4**. (a, c, e, g) Perspective view of the crystal structure (backbone only) of **H1**, **H2**, **H3**, and **H4**, showing 50% probability thermal ellipsoids. The angle between the two planes of the rings (θ_{AK}, θ_{EO}) is highlighted in red. (b, d, e, f) The packing arrangements in the crystal showing close π-π contacts between the two neighboring enantiomers. 3D packing structure in crystal with space-filling model (*M*- and *P*- enantiomers are colored in blue and magenta, respectively).

The structures of **H1**-**H4** were further characterized by ^{1}H NMR and ^{13}C NMR, and all the ^{1}H NMR peaks were assigned by 2D NOESY NMR technique (Figures S1-S4 in SI). Most of the protons on the π-conjugated skeleton appear at low field (δ = 8.0~13.0 ppm), except that the protons on the two terminal benzene rings show up-field shift due to spatial overlap (shielding effect) with the benzenoid rings in the neighboring layer, indicating that these expanded helicenes have localized aromatic character like kekulenes and cycloarenes.[9-11] This is further supported by nucleus-independent chemical shift, anisotropy of the induced current density, and 3D isochemical shielding surface calculations (Figures S21-S23 in SI). Accordingly, compounds **H1**-**H4** show similar UV-vis absorption spectra in DCM, with the absorption onset slightly red shifted with the extension of the molecular size (Figure 3). Time-dependent density functional theory (TD DFT) calculations suggest that the low-energy absorption band at about 440-500 nm can be correlated to the multiple HOMO−n→LUMO+m (n, m = 0−2) electronic transitions (Tables S5-S8 in SI). These four compounds also show similar fluorescence spectra, with a slight red shift of the emission maximum (487, 505, 514 and 519 nm for **H1**, **H2**, **H3** and **H4**, respectively) with the extension of length (Figure 3). The absolute photoluminescence quantum yields (PLQYs) of **H1**, **H2**, **H3**, and **H4** in DCM were determined to be 21.0%, 19.1%, 18.9%, and 16.6%, respectively, by using integrating sphere technique. The relatively low PLQYs can be explained by the nearly forbidden HOMO→LUMO electronic transitions (*f* = 0, 0.030, 0.025, 0.030, respectively, according to TD DFT calculations). Furthermore, their corresponding fluorescence lifetimes (τ) were measured as 10.2, 12.8, 13.1 and 13.0 ns, respectively (Figure S6 in SI). Cyclic voltammetry measurements of the four expanded helicenes in DCM generally revealed multiple irreversible redox waves (Figure S7 in SI) due to the local aromatic character and large band gaps.

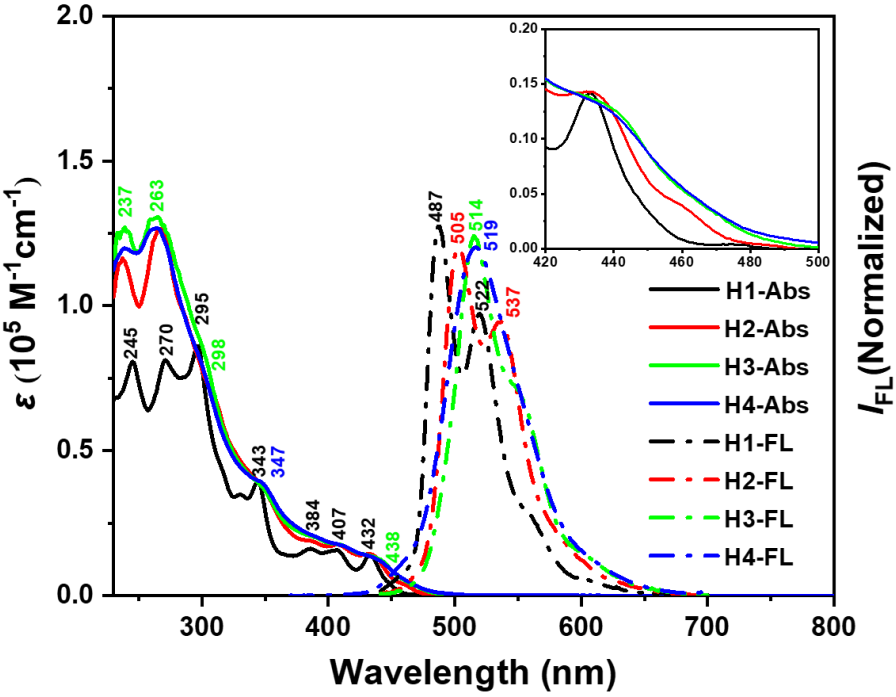

Figure 3. UV-vis absorption (Abs) and normalized fluorescence (FL) spectra of **H1**, **H2**, **H3**, and **H4** measured in DCM. The excitation wavelengths for FL are 350 nm. The inset shows the magnified absorption spectra at the long-wavelength region.

The racemic mixture of **H2**, **H3**, and **H4** can be resolved by chiral HPLC at room temperature. However, no separation was detected under any condition tested for **H1** due to its small racemization barrier (12.65 kcal/mol according to DFT calculations, Figure S19 in SI). The enantiomers of **H2** were separated by using a steroid-loaded silica gel column under HPLC conditions (eluent: 40% MeCN/DCM) to give (−)400-**H2** and (+)400-**H2** (Figure S8 in SI). The enantiomers, (−)400-**H3**/(+)400-H3 and (−)400-**H4**/(+)400-**H4**, were separated under similar conditions (**H3**: 50% MeCN/DCM, **H4**: 52% MeCN/DCM). All the circular dichroism (CD) spectra of enantiomers are complete mirror images (Figure 4a), and the absolute configurations are assigned as (+)400 = (*P*)/(−)400 = (*M*), based on experimental and theoretical CD spectra (Figure S9 in SI). Positive Cotton effects (CEs) between 354-500 nm for (*P*)-**H2**, 347-500 nm for (*P*)-**H3** and 344-500 nm for (*P*)-**H4** are observed, while strong negative CEs are found in the ranges of 254-354 nm for (*P*)-**H2**, 253-347 nm for (*P*)-**H3** and 250-344 nm for (*P*)-**H4**. It is worth noting that **H2**, **H3**, and **H4** show $|g_{abs}|$ maxima of up to 0.020 at 420 nm, 0.021 at 421 nm and 0.024 at 451 nm, respectively, which are among the highest values for helicenes and helicene-like structures in the visible range.

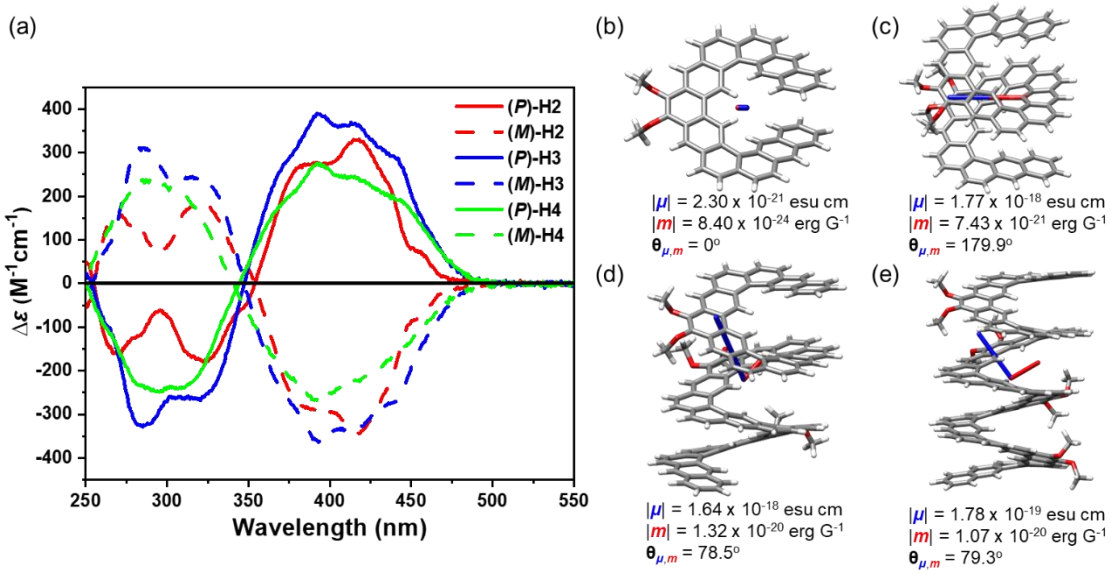

Figure 4. (a) CD spectra of (*P*)-**H1**, (*M*)-**H1**, (*P*)-**H2**, (*M*)-**H2**, (*P*)-**H3**, (*M*)-**H3**, (*P*)-**H4**, (*M*)-**H4**, measured in DCM at room temperature with different concentrations (c = 5.79 × 10^{-6} M, 6.46 × 10^{-6} M, 4.69 × 10^{-6} M, 5.99 × 10^{-6} M, 5.14 × 10^{-6} M, 4.08 × 10^{-6} M, respectively). (b, c, d, e) Calculated transition dipole moments for the S0→S1 electronic transitions in (*M*)-**H1**, (*M*)-**H2**, (*M*)-**H3**, (*M*)-**H4**. The electric transition dipole moments (***μ***) are shown in blue, and the magnetic transition dipole moments (***m***) are shown in red. Arrows for moments are displayed with 1 a.u. = 4 Å.

To understand the origin of the high $|g_{abs}|$ values, transition dipole moments and chiroptical properties were also investigated. According to theory, the dissymmetry factors can be calculated by the equation $g = 4\cos\boldsymbol{\theta}|\boldsymbol{m}||\boldsymbol{\mu}|/(|\boldsymbol{m}|^2+|\boldsymbol{\mu}|^2)$, wherein ***μ***, ***m***, and ***θ*** represent the electric and magnetic transition dipole moments, as well as the angle between ***μ*** and ***m***, respectively.[17] For organic materials, the $|\boldsymbol{m}|$ value is normally much

lower than the $|\boldsymbol{\mu}|$ value. The above equation can thus be simplified as $g = 4\cos\boldsymbol{\theta}|\boldsymbol{m}|/|\boldsymbol{\mu}|$. Calculation suggests that with the extension of the molecular size, the $|\boldsymbol{m}|$ values for the S0-S1 transition increase from **H1** to **H3**, presumably due to more effective π-electron delocalization (Figure 4b-d). However, the value slightly drops at **H4**, indicating the saturation of effective conjugation, which is in agreement with the frontier orbital profile analysis (Figures S11, S13, S15, S17 in SI). It is also found that the $\boldsymbol{\theta}$ angle strongly depends on the molecular symmetry, that is, for **H1** and **H2**, the $\boldsymbol{\mu}$ and $\boldsymbol{m}$ are almost aligned along one line, while for **H3** and **H4**, large $\boldsymbol{\theta}$ angles (nearly 80°) are calculated. The calculated absorption dissymmetry factors g_{cal} (**H1**: 0.015, **H2**: 0.017, **H3**: 0.006, and **H4**: 0.045) are consistent with the trend observed experimentally.

In summary, a facile synthetic strategy involving $Bi(OTf)_3$-catalyzed cyclization reaction of vinyl ethers was developed for the synthesis of a series of expanded helicenes in a nearly "one-pot" mode. The obtained helical polyarenes contain up to 35 cata-fused benzene rings which represent a record for helicenes and expanded helicenes. Notably, enantiopure **H2**, **H3**, and **H4** can be isolated, and they all show strong chiroptical responses with relatively large $|g_{abs}|$ values (up to 0.024). Further improvement of both dissymmetric factors as well as fluorescence quantum yield is possible by adjusting the building blocks and molecular symmetry via the same synthetic method.

Notes

The authors declare no competing financial interest.

Acknowledgements

J.W. and S.W. acknowledge the financial support from A*STAR AME IRG grant (A20E5c0089), AME YIRG grant (A2084c0164) and NRF Investigatorship award (NRF-NRFI05-2019-0005). H.I. and T.M.F. thank the financial support from KAKENHI (20H05672 and 22K20527). We also thank Prof. D. Jiang and Dr. S. Tao in NUS for the help on the absolute fluorescence quantum yield measurements.

References

(1) (a) A. Urbano, *Angew. Chem. Int. Ed.* **2003**, *42*, 3986; *Angew. Chem.* **2003**, *115*, 4116. (b) Y. Shen, C. -F. Chen, *Chem. Rev.* **2012**, *112*, 1463. (c) M. Gingras, *Chem. Soc. Rev.* **2013**, *42*, 968. (d) M. Gingras, G. Félix, R. Peresutti, *Chem. Soc. Rev.* **2013**, *42*, 1007. (e) M. Gingras, *Chem. Soc. Rev.* **2013**, *42*, 1051. (f) C. -F. Chen, Y. Shen, Helicene Chemistry, Springer, Berlin, Heidelberg, **2017** (g) I. G. Stará, I. Starý, *Acc. Chem. Res.* **2020**, *53*, 144. (h) M. Jakubec, J. Storch, *J. Org. Chem.* **2020**, *85*, 13415. (i) J. Crassous, I. G. Stará, I. Starý, Helicenes - Synthesis, Properties and Applications, Wiley, **2022**.

(2) K. Mori, T. Murase, M. Fujita, *Angew. Chem. Int. Ed.* **2015**, *54*, 6847; *Angew. Chem.* **2015**, *127*, 6951.

(3) See reviews: (a) C. Li, Y. Yang, Q. Miao, *Chem. Asian J.* **2018**, *13*, 884. (b) J. M. Fernández-García, P. J. Evans, S. Filippone, M. Á. Herranz, N. Martín, *Acc. Chem. Res.* **2019**, *52*, 1565. (c) T. Mori, *Chem. Rev.* **2021**, *121*, 2373. See representative examples: (d) T. Fujikawa, Y. Segawa, K. Itami, *J. Am. Chem. Soc.* **2015**, *137*, 7763. (e) T. Fujikawa, Y. Segawa, K. Itami, *J. Am. Chem. Soc.* **2016**, *138*, 3587. (f) L. L. Zhou, M. Li, H. Y. Lu, C. F.

Chen, *Polym. Chem*. **2016**, *7*, 310. (g) Y. Hu, X. -Y. Wang, P.-X. Peng, X. -C. Wang, X. -Y. Cao, X. Feng, K. Müllen, A. Narita, *Angew. Chem. Int. Ed.* **2017**, *56*, 3374; *Angew. Chem.* **2017**, *129*, 3423. (h) T. Hosokawa, Y. Takahashi, T. Matsushima, S. Watanabe, S. Kikkawa, I. Azumaya, A. Tsurusaki, K. Kamikawa, *J. Am. Chem. Soc.* **2017**, *139*, 18512. (i) K. Kato, Y. Segawa, L. T. Scott, K. Itami, *Angew. Chem. Int. Ed*. **2018**, *57*,1337; *Angew. Chem.* **2018**, *130*, 1351. (j) Y. Zhu, Z. Xia, Z. Cai, Z. Yuan, N. Jiang, T. Li, Y. Wang, X. Guo, Z. Li, S. Ma, et al., *J. Am. Chem. Soc.* **2018**, *140*, 4222. (k) H. Tanaka, Y. Kato, M. Fujiki, Y. Inoue, T. Mori, *J. Phys. Chem. A* **2018**, *122*, 7378. (l) B. Liu, M. Böckmann, W. Jiang, N. L. Doltsinis, Z. Wang, *J. Am. Chem. Soc.* **2020**, *142*, 7092. (m) X. Jiang, S. D. Laffoon, D. Chen, S. Pérez-Estrada, A. S. Danis, J. Rodríguez-López, M. A. Garcia-Garibay, J. Zhu, J. S. Moore, *J. Am. Chem. Soc.* **2020**, *142*, 6493. (n) N. J. Schuster, L. A. Joyce, D. W. Paley, F. Ng, M. L. Steigerwald, C. Nuckolls, *J. Am. Chem. Soc.* **2020**, *142*, 7066. (o) X. Xiao, S. K. Pedersen, D. Aranda, J. Yang, R. A. Wiscons, M. Pittelkow, M. L. Steigerwald, F. Santoro, N. J. Schuster, C. Nuckolls, *J. Am. Chem. Soc.* **2021**, *143*, 983. (p) J. -K. Li, X. -Y. Chen, Y. -L. Guo, X. -C. Wang, A. C. -H. Sue, X. -Y. Cao, X. -Y. Wang, *J. Am. Chem. Soc.* **2021**, *143*, 17958. (q) Y. Nakakuki, T. Hirose, H. Sotome, M. Gao, D. Shimizu, R. Li, J. Y. Hasegawa, H. Miyasaka, K. Matsuda, *Nat. Commun.* **2022**, *13*, 1475.

(4) G. R. Kiel, S. C. Patel, P. W. Smith, D. S. Levine, T. D. Tilley, *J. Am. Chem. Soc.* **2017**, *139*, 18456.

(5) (a) K. Fujise, E. Tsurumaki, G. Fukuhara, N. Hara, Y. Imai, S. Toyota, *Chem. Asian J.* **2020**, *15*, 2456. (b) H. Kubo, T. Hirose, T. Nakashima, T. Kawai, J. -Y. Hasegawa, K. Matsuda, *J. Phys. Chem. Lett.* **2021**, *12*, 686. (c) M. Hasegawa, Y. Nojima, Y. Mazaki, *ChemPhotoChem* **2021**, *5*, 1042.

(6) Y. Nakakuki, T. Hirose, K. Matsuda, *J. Am. Chem. Soc.* **2018**, *140*, 15461.

(7) K. Fujise, E. Tsurumaki, K. Wakamatsu, S. Toyota, *Chem. Eur. J.* **2021**, *27*, 4548.

(8) W. Zheng, T. Ikai, K. Oki, E. Yashima, *Nat. Sci.* **2022**, *2*: e20210047.

(9) W. Fan, Y. Han, S. Dong, G. Li, X. Lu, J. Wu, *CCS Chem.* **2020**, *2*, 1445.

(10) W. Fan, Y. Han, X. Wang, X. Hou, J. Wu, *J. Am. Chem. Soc*. **2021**, *143*, 13908.

(11) W. Fan, T. Matsuno, Y. Han, X. Wang, Q. Zhou, H. Isobe, J. Wu, *J. Am. Chem. Soc.* **2021**, *143*, 15924.

(12) X. Lu, T. Y. Gopalakrishna, H. Phan, T. S. Herng, Q. Jiang, C. Liu, G. Li, J. Ding, J. Wu, *Angew. Chem. Int. Ed.* **2018**, *57*; *Angew. Chem.* **2018**, *130*, 13236.

(13) S. Saito, H. Yamaguchi, H. Muto, T. Makino, *Tetrahedron Lett.* **2007**, *48*, 7498.

(14) C. Liu, M. E. Sandoval-Salinas, Y. Hong, T. Y. Gopa-lakrishna, H. Phan, N. Aratani, T. S. Herng, J. Ding, H. Yamada, D. Kim, D. Casanova, J. Wu, *Chem* **2018**, *4*, 1586.

(15) Crystallographic data for **H1**, **H2**, **H3** and **H4** are deposited in the Cambridge Crystallographic Data Center with number 2212268, 2212270, 2212280 and 2212271, respectively.

(16) J. B. Birks, D. J. S. Birch, E. Cordemans, E. V. Donckt, *Chem. Phys. Lett.* **1976**, *43*, 33.

(17) (a) J. A. Schellman, *Chem. Rev.* **1975**, *75*, 323. (b) F. S. Richardson, J. P. Riehl, *Chem. Rev.* **1977**, *77*, 773. (c) S. Sato, A. Yoshii, S. Takahashi, S. Furumi, M. Takeuchi, H. Isobe, *Proc. Natl. Acad. Sci. USA* **2017**, *114*, 13097. (d) Z. Qiu, C. -W. Ju, L. Frédéric, Y. Hu, D. Schollmeyer, G. Pieters, K. Müllen, A. Narita, *J. Am. Chem. Soc.* **2021**, *143*, 4661.